catalysts

MDPI

Article

Environmental Impacts on the Photocatalytic Activities of Anatase and Rutile

Karolina Solymos [1,2], Áron Ágoston [1,3], Tamás Gyulavári [1], Lilla Szalma [1], Milica Todea [4,5], Ákos Kukovecz [1], Zoltán Kónya [1] and Zsolt Pap [1,5,6,*]

1 Department of Applied and Environmental Chemistry, University of Szeged, Rerrich Béla Sqr. 1, H-6720 Szeged, Hungary; solymoskarolina@geo.u-szeged.hu (K.S.); agostona@chem.u-szeged.hu (Á.Á.); gyulavarit@chem.u-szeged.hu (T.G.); szlili566@gmail.com (L.S.); kakos@chem.u-szeged.hu (Á.K.); konya@chem.u-szeged.hu (Z.K.)
2 Department of Physical and Environmental Geography, University of Szeged, Egyetem Str. 2–6, H-6722 Szeged, Hungary
3 Department of Physical Chemistry and Materials Sciences, University of Szeged, Rerrich B. Sqr. 1, H-6720 Szeged, Hungary
4 Faculty of Medicine, Iuliu Haţieganu University of Medicine and Pharmacy, Victor Babeş 8, 400012 Cluj-Napoca, Romania; todeam@phys.ubbcluj.ro
5 Nanostructured Materials and Bio-Nano-Interfaces Center, Interdisciplinary Research Institute on Bio-Nano-Sciences, Babes-Bolyai University, T. Laurian 42, 400271 Cluj-Napoca, Romania
6 Centre for 3B, Babeş–Bolyai University, Clinicilor 5-7, 400006 Cluj-Napoca, Romania
* Correspondence: pzsolt@chem.u-szeged.hu; Tel.: +36-62-543-795

Abstract: Titanium dioxide (TiO_2) nanoparticles (NPs) are widely used in various industries and are increasingly found in environmental systems, especially in soil. However, the environmental behavior of TiO_2 NPs is still poorly understood. Hence, this study aims to fill this gap by investigating the short- and long-term effects of soil solutions on anatase and rutile NPs. The experiments were carried out using two soil types, which have very different chemical properties, in order to obtain a more nuanced picture of how these factors affect the stability, surface chemistry, and photocatalytic activity of TiO_2 NPs. The results indicate that acidic soil solutions with lower ionic strength tend to enhance the stability of TiO_2 NPs by preventing aggregation, while alkaline solutions with higher ionic strength promote aggregation and reduce photocatalytic activity by blocking active sites. Additionally, the adsorption of organic matter and other soil components on the nanoparticle surface further complicates their behavior, potentially reducing their photocatalytic efficiency. The interaction time plays a crucial role in determining the long-term fate of TiO_2 NPs in soil environments. Extended exposure to soil solutions leads to changes in crystallite size, surface charge, and the adsorption of functional groups, which, in turn, affect the NPs' photocatalytic properties.

Keywords: titania; soil solution; photocatalytic activity; interaction time

Academic Editor: Nina Kaneva

Received: 20 January 2025
Revised: 13 February 2025
Accepted: 14 February 2025
Published: 18 February 2025

Citation: Solymos, K.; Ágoston, Á.; Gyulavári, T.; Szalma, L.; Todea, M.; Kukovecz, Á.; Kónya, Z.; Pap, Z. Environmental Impacts on the Photocatalytic Activities of Anatase and Rutile. *Catalysts* **2025**, *15*, 190. https://doi.org/10.3390/catal15020190

1. Introduction

Titanium dioxide (TiO_2) is a highly recognized material for its extensive applications in various fields, including photocatalysis [1] (air [2] and water purification [3], as well as self-cleaning surfaces [4]); pigment production [5]; cosmetics industry [6]; agriculture [7]; and in energy conversion as solar batteries [8]. The TiO_2 market is expected to develop at a compound annual growth rate (CAGR) of 6.3% from 2023 to 2030, and it was valued at around 19 billion USD in 2022 [9].

TiO_2 primarily occurs in three crystalline forms: anatase, rutile, and brookite [10]. Anatase, alongside rutile, is a stable polymorph of TiO_2 and is widely utilized as a photocatalyst or catalyst support due to its favorable properties. Anatase typically offers higher specific surface areas compared to rutile, making it particularly valuable for (photo)catalytic applications [11]. Rutile, with a band gap of approximately 3.0 eV, generally exhibits lower photocatalytic activity than anatase [12]. However, there are exceptions where rutile can exhibit a higher specific surface area than anatase, depending on the synthesis methods and conditions [13]. Brookite, on the other hand, has limited research on its photocatalytic properties, likely due to the challenges associated with producing this material in high purity [14].

Due to the widespread application and high accumulation rate of titania, its environmental concentration is constantly increasing [15]. Sources of environmental release include industrial effluents, runoff from agricultural lands treated with TiO_2-containing products [16], washing down from the self-cleaning surfaces [17], and also the degradation of consumer goods [18]. Once in the environment, TiO_2 nanoparticles (NPs) can enter soil systems, where they may interact with soil components and impact both the abiotic and biotic elements of these ecosystems [19].

Several studies have demonstrate the human [20] and ecotoxicological effects of TiO_2, and, even at low concentrations, TiO_2 has negative effects on soil microbial activity [21]. It can be transferred to the growing plants by their roots, so, if released on agricultural land, it can enter the food chain [22]. This could be of serious concern as TiO_2 has been classified as a carcinogen by the International Agency for Research on Cancer (IARC) [23]. In addition, research has shown that it can also affect the ecological behavior patterns of the insects living in the soil [24]. Certainly, the toxicological impact, and generally the behavior and fate of TiO_2 in the soil, can be influenced by a number of factors like pH, ionic strength, and the dissolved organic matter content [25].

Central to understanding the interactions is the soil solution, which refers to the liquid phase within the soil containing dissolved organic and inorganic substances [26]. The basic property of a soil solution is that it brings some of the constituents of the inert solid phase into an available, reactive form (e.g., dissolves or hydrolyses), thereby "revitalising" the soil. The properties of the soil are therefore determined by the substances present in the soil solution [27]. When TiO_2 NPs are introduced into the soil, they can disperse into the soil solution through various mechanisms such as leaching and runoff. This dispersion into the soil solution is a critical pathway through which TiO_2 NPs interact with soil components and potentially influence the soil's balance and health [28].

It is significant to highlight that the majority of studies focused on how TiO_2 NPs behave in aqueous conditions or in the solid phase of soil. To the best of our knowledge, little is known about how soil solutions affect these materials. For this reason, this study presents comparative analyses of TiO_2 polymorphs, both anatase and rutile, and their interactions within different soil environments.

For this reason, Regosol and Solonetz soil types were chosen for this study based on the World Reference Base for Soil Resources (WRB). Regosol, which makes up around 2% of the continent, is mostly found on hill slopes in Eastern Europe, the Middle East, and Northern China. It is distinguished by its reddish-brown color, sand texture, and high organic matter content [29]. Known for its alkaline character and salt buildup, Solonetz, which makes up around 1% of continental land, flourishes in the dry temperatures of North America, Northern Asia, and Central Asia [30]. Additionally, these soil types are representative of the Hungarian soil environment, making them particularly relevant for our study. The selection was also motivated by the need to cover a broad spectrum of

chemical compositions to better understand the behavior of TiO_2 NPs under different geochemical conditions.

Therefore, the aim of this study was to fill an important gap in our understanding of how soil solution properties can affect the behavior of TiO_2 NPs, including their photocatalytic activity, in both the short and long term. The approach taken in this study allowed us to evaluate not only their direct interactions with soil components, but also their longer-term stability, surface chemical changes, and photocatalytic efficiency. The novelty of this work can lie in the fact that, by comprehensively investigating the immediate and long-term effects of TiO_2 in soil solutions, it provides new insights that can enrich and change our understanding of their environmental behavior and applications.

2. Results and Discussion

2.1. Properties of Soil Solutions and Their Possible Effects on TiO_2 NPs

In order to obtain an overall picture of the effect of soil solutions on the behavior of TiO_2 NPs, different physicochemical parameters of the soil solutions were also investigated (Table 1).

Table 1. Chemical properties of the soil solutions.

Parameters		REGOSOL Soil Solution (REG)	SOLONETZ Soil Solution (SOL)
pH		4.9 ± 0.1	9.4 ± 0.2
IS (mmol·L^{-1})		2 ± 0.1	12 ± 0.3
TOC	mg·L^{-1}	91.1 ± 1.2	72.4 ± 1.6
Na		2.6 ± 0.3	73.4 ± 1.1
K		38.4 ± 0.8	34.5 ± 1.8
Ca		32.6 ± 0.1	82.7 ± 0.4
Mg		9.8 ± 0.2	26.4 ± 0.3
NO_3		21.6 ± 0.1	24.6 ± 0.2
PO_4		1.3 ± 0.2	0.7 ± 0.1
F		0.1 ± 0.02	0.5 ± 0.1
Cl		3.5 ± 0.5	15.5 ± 0.4
SO_4		1.7 ± 0.2	4.6 ± 0.6
Al		9.8 ± 0.5	5.7 ± 0.3
Fe		3.2 ± 0.1	1.4 ± 0.2

The pH values of the soil solutions varied significantly: the average pH of the Regosol soil solution (REG) was ~4.95 (acidic), whereas the Solonetz soil solution (SOL) had an average pH of ~9.44 (strongly alkaline). It is known that pH significantly impacts the catalysts' isoelectric point (IEP) and ζ potential.

In acidic media, the surface of the material may become positively charged due to the excess H^+, promoting the adsorption of various anions [31]. However, this is not necessarily an occurring phenomenon as the soil solution is a complex chemical system and because numerous other components can influence the surface charge of the particles.

In an alkaline medium, the excess OH^- causes the opposite scenario, potentially leading to the adsorption of mainly cations on the surface [32].

The IS of the two soil solutions also differed significantly. The SOL had a very high IS (12 mmol·L^{-1}), which can reduce the electrostatic repulsion between NPs, making them more prone to aggregation. However, a high IS can also negatively affect the photocatalytic activity of TiO_2 by blocking active sites [33]. In contrast, when there is a REG with low IS (2 mmol·L^{-1}), then the dominant factor is the electrostatic repulsion between charged NPs. This repulsion helps prevent aggregation and stabilizes the colloidal suspension [28,34].

The organic matter content in an aqueous medium is represented by the TOC values. The TOC contents of the two soil solutions were not significantly different from one another; both had high values (Table 1), with the one measured for REG being the higher one (91.1 $mg \cdot L^{-1}$). TiO_2 NP's photocatalytic activity is significantly impacted by its high organic matter content because different organic molecules can be adsorbed onto its surface and obstruct access to its active sites [35]. This makes it more difficult for the photocatalyst and the intended contaminants or substrates to interact. Furthermore, the target pollutants and organic molecules could compete for the available adsorption sites on the surface of TiO_2. Higher surface affinity for the organic molecules allows them to efficiently displace the target pollutants, reducing the amount of photocatalytic activity directed toward those pollutants [36].

In both soil solutions, there were low amounts of Fe (3.2 $mg \cdot L^{-1}$ in the case of REG, while 1.4 $mg \cdot L^{-1}$ for SOL) and Al (9.8 $mg \cdot L^{-1}$ for REG and 5.7 $mg \cdot L^{-1}$ for SOL) were detected. The adsorption of Fe on the surface has been shown in several studies to be able to alter the optical properties of the materials and thus to be able to absorb light more efficiently in the visible light spectrum [37–39]. However, there are exceptions, with some studies showing that the presence of Fe can also inhibit the activity of TiO_2, depending on the mode of synthesis [40]. Al, although not what is classically known as a catalyst "poison", can indirectly affect recombination through its surface adsorption, thus influencing the activity of the material [37]. Significant amounts of Cl^- were measured, especially in the SOL soil solution. Cl was able to adsorb on the TiO_2 surface, forming surface complexes. This may reduce the activity as Cl ions can block the active sites, altering the surface charge. In addition, Cl may compete for the catalyst surface with other species [41].

Certain ions in soil solutions were also tested since their presence can influence the behavior of TiO_2. The SOL soil solution's concentrations of Na and Ca were high and low for REG (Table 1). For TiO_2 NPs in an aquatic medium, some publications have observed enhanced sedimentation and aggregation at levels comparable to SOL [42,43].

Significant amounts of various anions were measured in both soil solutions, with Cl^- and SO_4 being prominent in SOL. Without exception, these anions are able to strongly adsorb on the surface of the material, occupying the active sites and thus reducing the catalytic activity. Of course, the surface adsorption of these anions is strongly influenced by the surface charge and the pH of the medium [44].

In addition to the previously listed factors, the TiO_2 NPs' behavior and photocatalytic activity in soil solutions can also be affected by their size, shape, surface chemistry, and crystal structure. The next sections will discuss these issues.

2.2. Morphology and Crystal Structure of TiO_2 NPs After Immersion in the Soil Solutions

The SEM micrographs show that both anatase and rutile have polycrystalline structures and that their particles form aggregates (Figure 1). After interaction with soil solutions, no visually significant changes in morphology were observed, and the degree of aggregation remained similar. For the AR_SOL_7 sample, however, an interesting observation can be made: the particles seemed to have been fragmented into smaller components. There may be several reasons for this; for example, the high ion content of a SOL soil solution can trigger reactions that weaken the rutile surface and potentially lead to fragmentation. Since rutile fragmentation did not occur after interaction with the acidic REG soil solution, the contribution of high alkaline pH could not be ruled out. However, this phenomenon was not observed in the AR_SOL_4 sample, suggesting that the time of interaction is also an important factor.

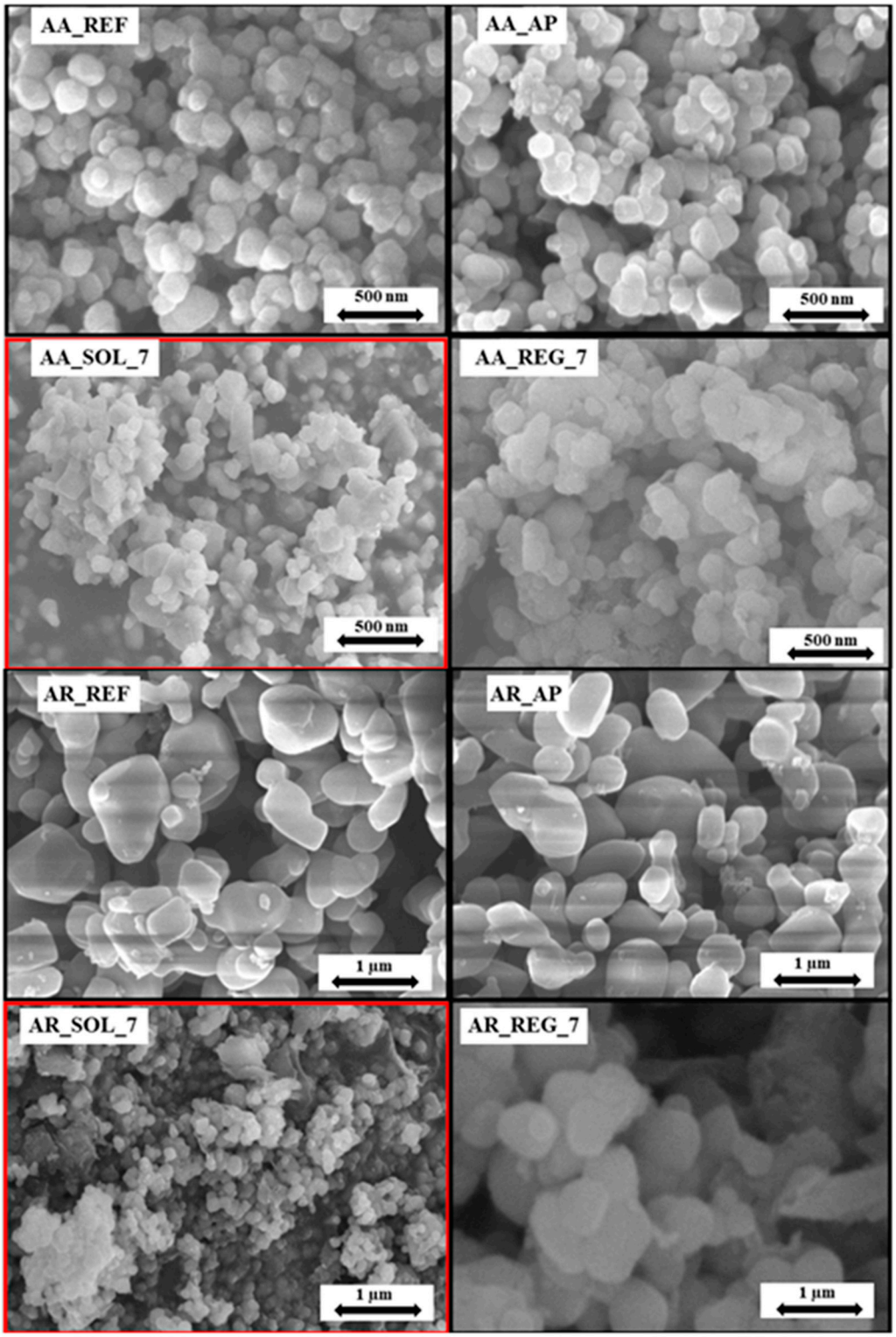

Figure 1. SEM micrographs of the samples and their changes in sizes (AA_SOL_7 and AR_SOL_7 (red framed)).

One of the possible scenarios for the fragmentation could be the alkaline conditions during the interaction tests between the solonetz soil solution and titania. It is known that rutile can be solubilized in alkaline conditions. The degree of solubility exclusively depends on the strength of the basic media (K_b value). Even at mildly basic conditions (pH = 8–9), a few micromoles of titania can be solubilized [45], meaning that a solonetz soil extract, with a pH value of 9–10, is capable of solubilizing even more. However,

the formed water–soluble complexes are in equilibrium with the main phase of titania (Equation (1)); thus, a re-precipitation is always possible. This means that, at any given time, some particles dissolve and some particles are formed, hence causing a texture change within the samples (namely causing a direct fragmentation). The general solubilization reaction can be described as follows:

$$\begin{gathered} TiO_2(s) + 2H_2O \leftrightarrow Ti(OH)_4\ (aq) \\ Ti(OH)_4\ (aq) + H_2O \leftrightarrow Ti(OH)_5^- + H^+ \\ H^+ + OH^- \leftrightarrow H_2O. \end{gathered} \quad (1)$$

In addition to morphology, the crystal structure and primary crystallite size of the materials were also examined based on their XRD patterns (Figure 2a,b). The distinctive diffraction signals of AR_REF were found at 25.2° (101), 27.4° (101), 36° (101), and 39.1° (200) (JCPDS Card no. 21-1276), while, for AA_REF, they were found at 25.2° (101), 36.9° (103), 37.8° (004), and 38.5° (112) (JCPDS Card no. 21-1272) [46]. The primary crystallite size was approximately 39 nm for AA_REF and ~200–400 nm for AR_REF. However, it is important to note that, with a large crystal size (>100 nm), the uncertainty of the calculation can be significant.

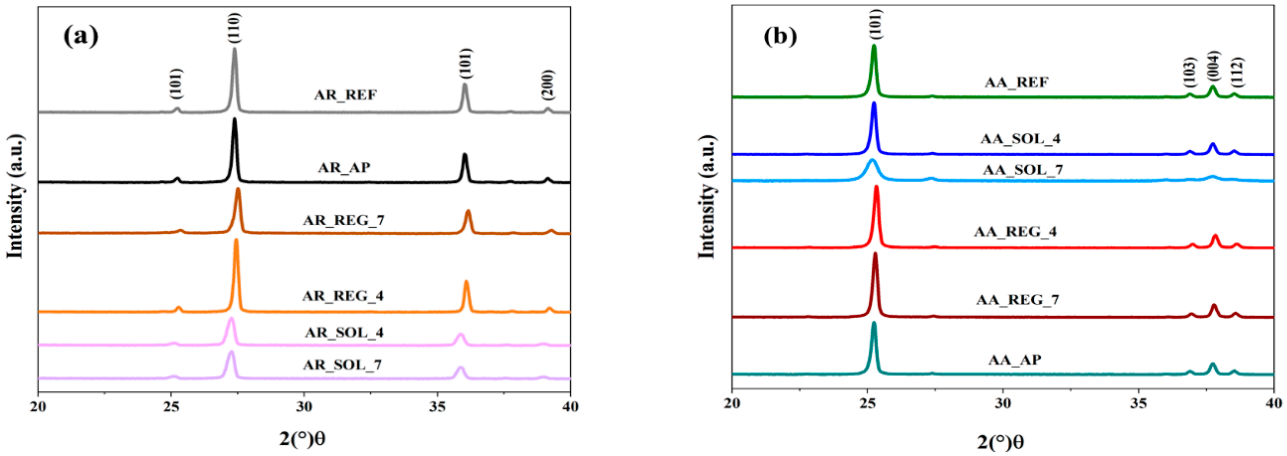

Figure 2. XRD patterns of the (**a**) Aldrich rutile samples before and after interaction with the soil solutions. (**b**) Aldrich anatase samples before and after interaction with the soil solutions.

After interaction with soil solutions, the primary crystallite size did not change in the materials; it was only below 5%, which is a negligible value. The XRD patterns show that no new diffraction peaks were formed and that the existing ones did not disappear after the interactions. The exception to this was AA_SOL_7, where the diffractogram showed a broadening of the peaks and a reduction in particle size to 32.4 nm (Figure 2b). Immersing in soil solutions may have caused some amorphization on the surface of the crystals, which manifested in the widening of the diffraction peaks. Additionally, for Samples AR_SOL_4 and AR_SOL_7, the broadening of the signals was also visible. Unfortunately, in this case, we could not determine the particle size from the XRD data due to methodological limitations. However, the SEM micrographs showed a spectacular reduction in size for the AR_SOL_7 sample.

2.3. Surface Properties

Through ζ potential measurements, we can obtain information from the particles' surface charge, which impacts the aggregation tendency and overall stability of the material [47]. These parameters could change depending on the soil solution's properties.

We also determined the IEP, or the pH of the zero net particle surface charge, in the soil solutions and, for comparison, in the distilled water as a reference (AA_REF and AR_REF).

For AA_REF, the IEP was around a pH of 2. After immersion in the acidic, low-ionic-strength, and high-organic-content Regosol soil solution (AA_REG), the material's IEP did not change. In contrast, in the alkaline, high-ionic-strength Solonetz soil solution (AA_SOL), the surface remained negatively charged across the measured pH range, as shown in Figure 3a. These highly extensive negative surface charges could be due to several reasons, but they were primarily due to components in the soil solutions. In AA_REG, most of the organic matter was adsorbed to the surface, which may have caused deprotonation. For example, carboxylic acids—the presence of which were also confirmed by the IR spectrum—can form carboxylate anions during deprotonation and drive the charge in a negative direction. In the case of AA_SOL, in addition to the quantity and quality of organic matter, even the high ion content may contribute. However, Ti-OH groups on the surface of material can also deprotonate [48].

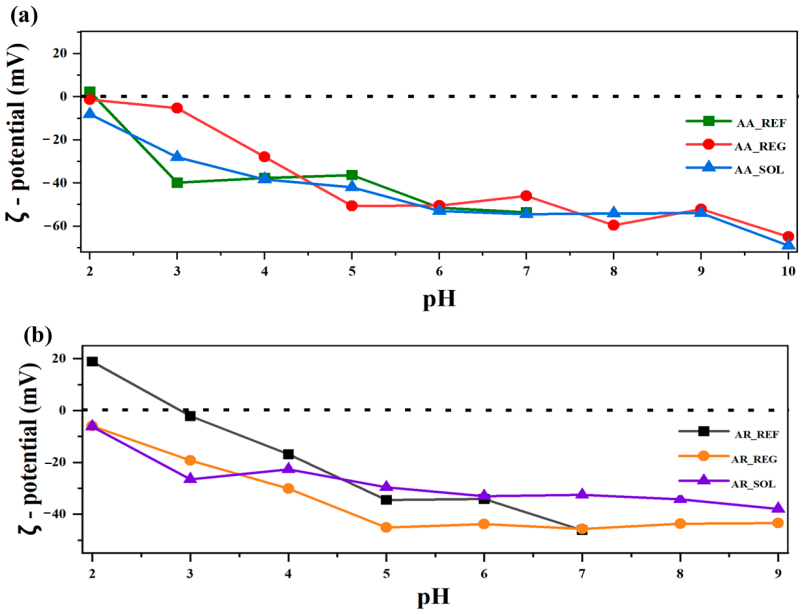

Figure 3. The ζ potential and IEP of the (**a**) Aldrich anatase and (**b**) Aldrich rutile samples in distilled water, as well as in Regosol and Solonetz soil solutions.

At the same time, such a negatively charged surface repels the anions in the solution and attracts the cations, which can lead to the formation of a double electrical layer [49].

For the AR samples, the IEP was a ~pH of 3, and the same trend was observed for AA: the ζ potential was in the same negative range when immersed in both soil solutions, and, like AA, with a few mV, the charge was more negative in acidic Regosol than in Solonetz (Figure 3b). Differences in the surface charge between the AA and AR samples can be attributed to the variances in their crystalline structure. The surface of anatase had more Lewis acidic Ti^{4+} centers, which are more prone to protonation (originating from the surface anchored OH groups), whereas the rutile structure had a lower proportion of these. This may explain the IEP of anatase at a lower pH [50]. Additionally, the difference in their surface arrangements and surface energy can influence the adsorption of ions. However, the specific surface of AA was also larger, so "more space is available" for the adsorption of various substances [12,51].

It is important to note that more intense IR peaks (Figures 4 and 5) were observed for AR than for AA. This suggests a higher adsorption of various substances, which may contribute to differences in ζ-potential. Although rutile typically has a smaller specific

surface area, its surface properties may allow for stronger or more selective adsorption of certain species from soil solutions.

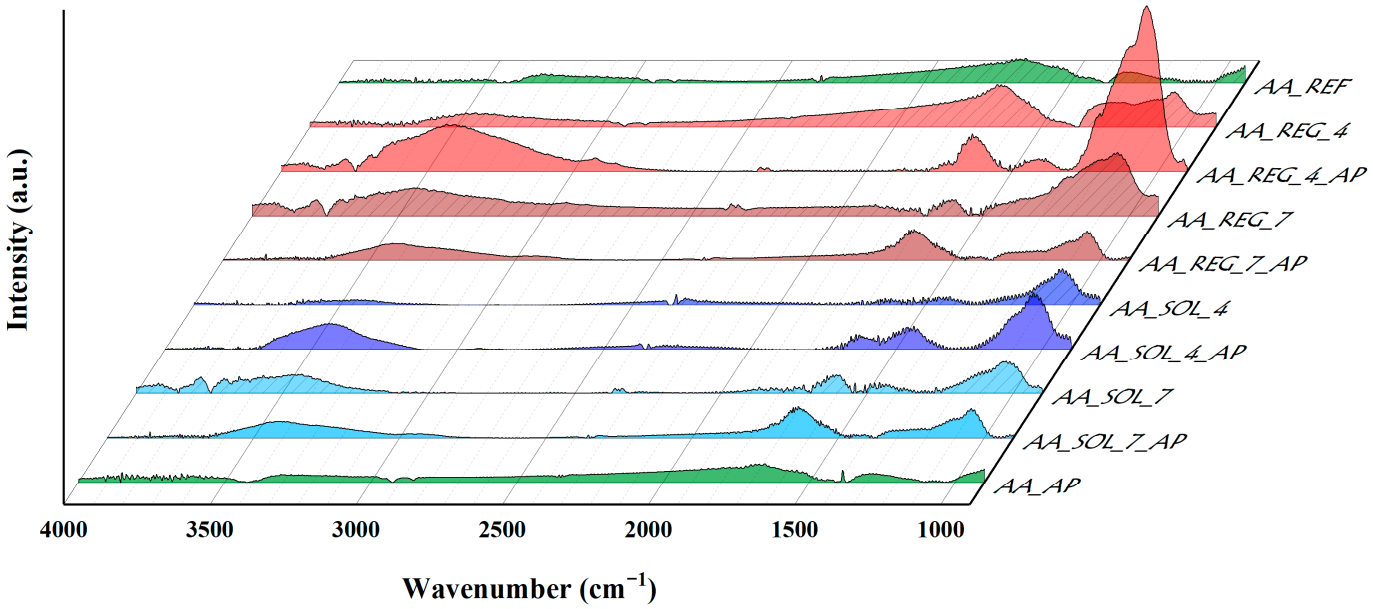

Figure 4. The IR spectra of the Aldrich anatase samples after interaction with the soil solutions in the 1000–4000 cm^{-1} region.

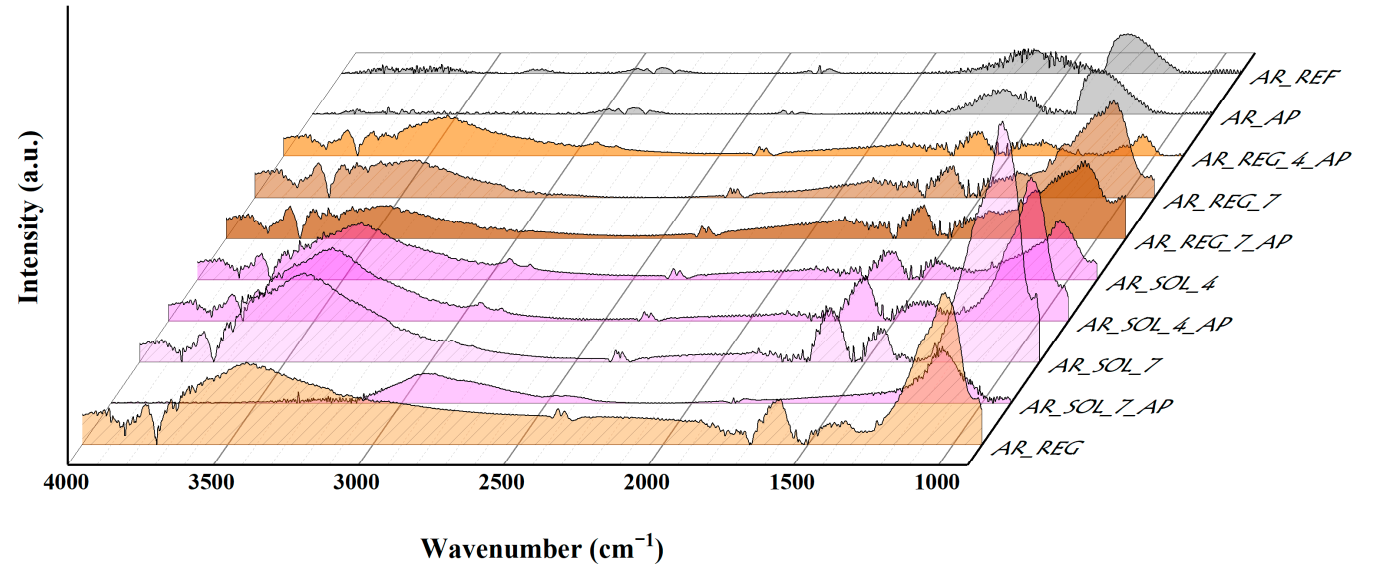

Figure 5. The IR spectra of the Aldrich rutile samples after interaction with the soil solutions in the 1000–4000 cm^{-1} region.

Following the surface properties, the types of vibrations corresponding to different functional groups were also identified based on IR spectra. These can provide key information about the surface chemical properties of NPs. These findings may help to understand the nature of surface interactions, such as the adsorption of organic compounds or the formation of surface complexes, which can affect the photocatalytic activity of NPs and, in general, their behavior in various complex environmental matrices.

Figures 4 and 5 display the samples' IR spectra. The primary constituents of the samples were metal oxides (Ti–O), which are represented by the bands at 400–900 cm^{-1}. There was no change in this region [52], so we normalized the spectra's other regions to

this. In every sample, vibration bands of CO_2 were detected at 2350 cm^{-1} [53]. These were unrelated to the analysis and came from the sample preparation procedure.

We also experienced lower or higher intensities for each sample in regions between 1000 and 1700 cm^{-1}. On the one hand, there was also a range of O-H vibration bands (1390, 1637–1650 cm^{-1}) [54,55]. For the AA_REF and AR_REF samples, this can be attributed to the presence of physisorbed water. In the case of AA_AP and AR_AP, the phenol model pollutant intermediates (e.g., hydroquinone, resorcinol, and pyrocatechol) [56,57] could be detected.

As can be seen in Figures 4 and 5, the samples interacting with soil solutions in this region had a much higher intensity than the reference samples. The bands were much "sharper" and more separable from each other, indicating the presence of other functional groups in addition to the O-H groups. For example, in the region between 1080 and 1150 cm^{-1}, there were Si-O vibrational bands [58]. This is because silicon oxides are prevalent in the soil as inorganic compounds, which are found in various minerals. Additionally, within the specific range of 1050 to 1100 cm^{-1}, we observed the vibrations of C-OH bonds [59]. These bonds are characteristic of oligosaccharides, which may originate from plant root remains [60]. Between 1250 and 1300 cm^{-1}, N-H bonds were detectable, which could be amides and amines. These may have been caused by the decomposition of the remains of various animal and plant organisms into the soil. In the 1360–1370 cm^{-1} range, vibrations of C-O bonds, which can be ascribed to long carbon-chain molecules in soil solutions (e.g., lignin-based substances from the decomposition of plants), and C-N bonds, which can be amides, amines, and imines, were detected. Between 1400 and 1420 cm^{-1}, there was an O-H region. These hydroxyl groups may be derived from carboxyl groups (from humic acid) in samples immersed in soil extracts. In the samples after phenol decomposition, phenol intermediates may also be present as O-H groups [59]. In the 1490–1500 cm^{-1} region, C=C vibrational bonds were found; these may be benzenoids, which are high molecular weight organic substances and may also be formed during the decomposition of animal residues.

In the 1580–1630 cm^{-1} region, there were the vibrations of N-H bonds, which represent the amine group and can come from peptides or even humic substances [61]. In the region around 3200 and 3600 cm^{-1}, there were vibrations of O-H bonds; this region is also known as the "water band", the presence of which has a strong influence on the hydrophilicity of a substance. As can be seen in the figures, for all samples (except AA_REF, AA_AP, AR_REF, and AR_AP), the "water band" was elevated [62]. It is also important to note that IR is a semi-quantitative method, and it is mainly suitable for qualitative determination, so we will not go into the details about the differences in intensity observed between the samples.

Overall, there was no significant difference between the soil extract-treated samples and the two types of TiO_2 in terms of which functional groups were adsorbed. There was no significant change in the bulk phase, as shown by the previous measurement techniques. However, the hydrophilicity of all samples increased. Furthermore, various long carbon chains, amines from peptides, and carboxylic acids were adsorbed on the surface of the materials. These observations may largely explain the changes in the photocatalytic activity of TiO_2 nanostructures.

Following their immersion in a soil solution, the surface composition of the photocatalysts was investigated using XPS measurements.

The elements clearly detected on the surface of the photocatalyst are shown in Table 2. Ti was found on all the sample surfaces, but its concentrations varied. The higher concentrations were clearly detected in the untreated samples (AA_REF and AR_REF).

Table 2. Surface chemical element composition based on XPS measurements.

Sample Name	Elemental Composition (a.m. %)										
	C	**O**	**Ti**	**Si**	**Al**	**Ca**	**Na**	**N**	**K**	**Cl**	**Fe**
AR_REF	51.5	36.2	11.9	n.d. [1]	n.d.	n.d.	n.d.	n.d.	n.d.	n.d.	n.d.
AR_REG_4	37.7	35.2	3.3	11.8	5.2	0.6	0.1	0.8	n.d.	0.4	4.9
AR_REG_7	26.7	41.1	0.8	22.2	7.3	0.8	n.d.	0.5	0.3	n.d.	0.2
AR_SOL_4	37.5	31	0.5	12.4	5.6	5.5	0.9	n.d.	n.d.	n.d.	6.6
AR_SOL_7	25.7	31.6	2.7	18.8	8.6	1.2	0.6	n.d.	0.5	n.d.	0.2
AA_REF	48.2	38	11.2	n.d.	n.d.	n.d.	n.d.	n.d.	n.d.	n.d.	n.d.
AA_REG_4	49	35.4	4.7	6.2	1.9	0.4	0.2	2	0.1	n.d.	n.d.
AA_REG_7	28.5	41.2	5.7	14.8	7.8	1.2	n.d.	0.4	0.4	n.d.	n.d.
AA_SOL_4	28.9	35.9	2.4	13.8	7.2	0.9	0.9	n.d.	0.3	n.d.	9.6
AA_SOL_7	31	32.7	2.7	11.5	6	0.7	0.8	n.d.	0.1	n.d.	14.4

[1] Not detected.

We detected C in very high proportions on the surface of AA_REF and AR_REF. This is a natural phenomenon that occurs when C is adsorbed from the atmosphere (i.e., different organic compounds) onto the material's surface. Carbon was also present in the IR spectra of all the samples, as indicated by the CO_2 region at 2350 cm^{-1}. After immersion in soil solutions, the C content decreased on the material's surface, partially due to the presence of other elements on the surface. However, with the exception of the AA_SOL samples (where the difference in C abundance between AA_SOL_4 and AA_SOL_7 was minimal and within the margin of error), the surface carbon abundance generally decreased with increasing interaction time. Since the samples were exposed to natural light during their interaction with the soil solutions, the photocatalytic activity of the materials was activated, leading them to "clean" the various organic substances from their surface. This hypothesis was confirmed for Sample AA_REG_7 by the decrease in the TOC content of the Regosol soil solution. The initial TOC concentration decreased from 91.1 $mg \cdot L^{-1}$ to 85.3 $mg \cdot L^{-1}$.

After immersion in the soil solutions, a significant amount of Si was detected on the surface of the materials, indicating the presence of SiO_2, which was confirmed by IR measurements. With increasing interaction time, the Si content also increased, except, in one case, for the AA_SOL sample group. The presence of this element can be explained by the fact that, since SiO_2 particles are positive and TiO_2 surfaces are negative in the ζ potential measurements, a strong electrostatic attraction occurs, which promotes the surface adsorption of SiO_2 particles. As the surface of the materials becomes C-depleted over time, it is better able to bind SiO_2. The same trend can be fully observed for Al. Significant amounts of this element were measured in soil solutions, and, as in the case of Si, the positively charged Al^{3+} ions and the negative surface of TiO_2 induced electrostatic attraction.

The relative oxygen content of the samples increased after interaction with the soil solutions when compared to the Ti surface content of the samples. This increase generally correlated with longer interaction times, except for the AA_SOL sample group again. The oxygen sequestration at the surface could be attributed to the presence of various organic matters, as supported by the IR results. Additionally, the increase in oxygen content could be also explained by the presence of SiO_2 because it showed a parallel increase with silicon over time.

Na, Ca, and K were detected on the surface of the materials at very low percentages. Despite their significant presence in the soil solutions, these cations were likely displaced from the surface by competing elements such as Si and Al. Nitrogen was also detected, potentially originating from various amine groups, in low amounts in the samples immersed in Regosol soil solution. Cl was found in a very small percentage and only on the surface

of one sample. No other anions, such as F, were detected, which could be attributed to the negatively charged surface.

For the AR samples, the amount of Fe in both acidic Regosol and alkaline Solonetz soil solutions decreased with increasing interaction time. For the AA_REG samples, no Fe was detected on the surface of the material, which could be due to the fact to the fact that Fe is highly soluble in acidic media [63]. In contrast, significant amounts of Fe were found at the surface in alkaline soil solutions, and the amount increased further with increasing interaction time.

2.4. Photocatalytic Activity

By measuring the rate of phenol degradation, the impact of soil solution on the photoactivity of AA and AR was examined. According to earlier adsorption research, the phenol adsorption on TiO_2 is quite small—between 2–4% [64]. Therefore, to guarantee that concentration variations result from catalytic degradation rather than adsorption, only a 10-minute dark period was used.

As can be seen in Figure 6a,b, after around 120 min of UV-A irradiation, AA_REF showed full phenol degradation. Compared to AA_REF, AR_REF (Figure 6c,d) was less effective; it took 180 min for the former catalyst to completely degradate the phenol.

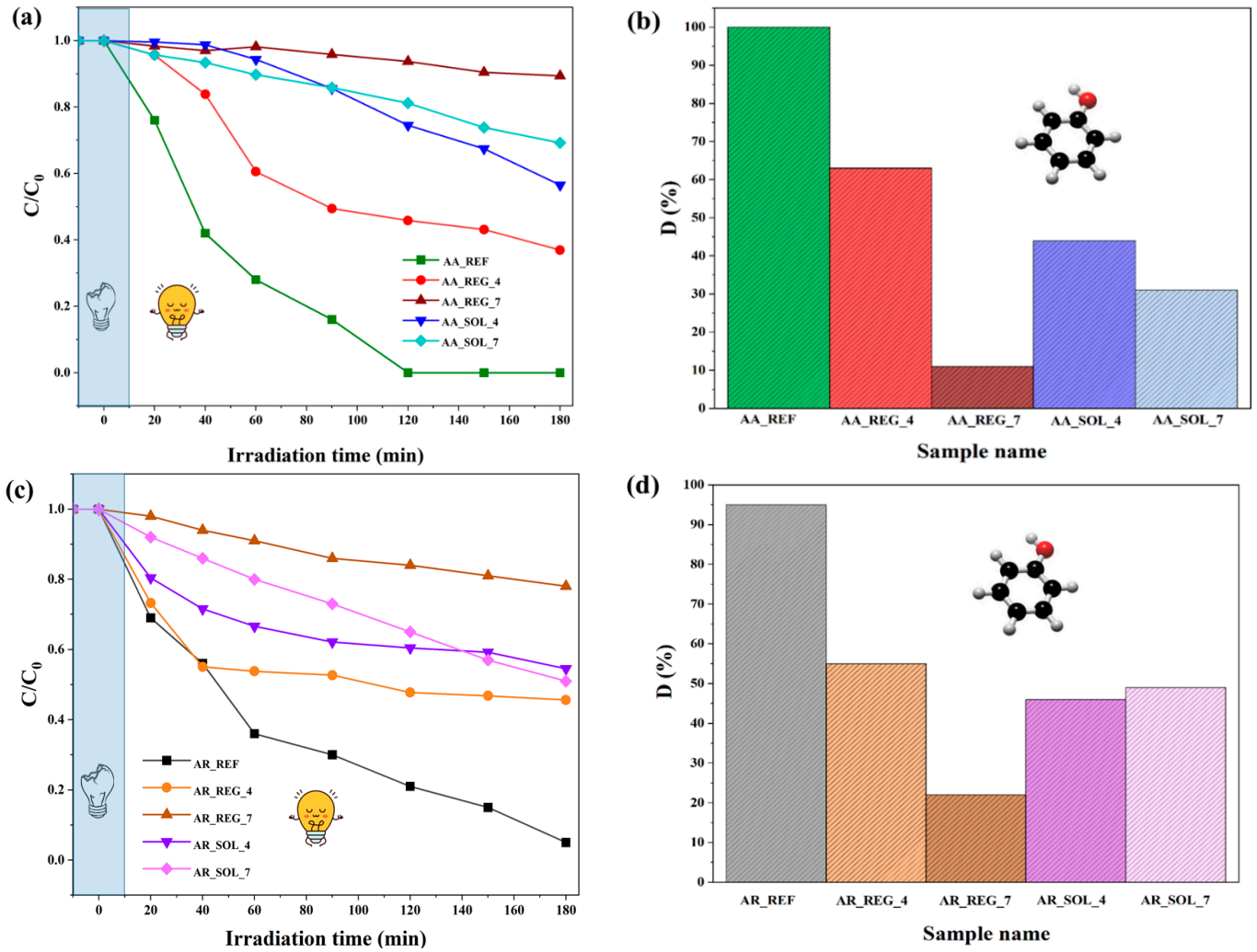

Figure 6. The phenol degradation curves of the (**a**) Aldrich anatase and (**c**) Aldrich rutile samples before and after interaction with soil solutions. The degradation percentage of the (**b**) Aldrich anatase and (**d**) Aldrich rutile samples.

Both the AA and AR samples showed a significant decrease in activity after interaction with REG soil solution. This became even more drastic after a longer interaction time. The decrease in activity was mainly due to the adsorption of the components from the soil solution onto the surface of the materials. The REG soil solution had a high TOC content, and the IR results confirmed that there were several organic components on the surface that hindered the accessibility of the active sites; thus, the activity was reduced. For example, humic acids can certainly form surface complexes on the surface of TiO_2 NPs as the carboxyl groups are able to complex with the surface metal centers of TiO_2. This interaction can lead to blocking of active sites, which reduces photocatalytic activity [65].

The XPS results showed that the amount of C and N decreased greatly with increasing interaction time. This led us to conclude that catalytic activity is taking place as AA and AR particles clean their surfaces. The reduced C and N content provided an opportunity for other components or elements to be released to the surface, which slowed down the activity to a large extent. These included Al and Si, whose presence and increase with interaction time were confirmed by the XPS results. These two elements have also been shown in previous studies to negatively affect the activity of catalysts [37].

In addition, Na and Ca were detected in both the AA_SOL and AR_SOL sample groups based on the XPS results. Both ions significantly affected the surface charge and activity of TiO_2, as well as, basically, the stability of the material. Na mainly affected the structure of the double electric layer, while the Ca was able to bind more strongly to the surface, neutralizing the charge and promoting aggregation [66]. Aggregation can reduce the availability of active sites, and Ca ions can also form surface complexes that can act as electron traps [67].

The AA_SOL samples showed the same trend as the AA_REG samples: activity decreases after interaction with the soil solution. This only increased after a longer interaction time. The SOL soil solution also had a high TOC content, so this may have also influenced the activity. With increasing interaction time, the XPS results showed an increase in Fe on the surface, which may have also decreased the activity [40].

The AR_SOL samples showed the opposite behavior to the previous set of samples as the activity improved with increasing interaction time (Figure 6d). However, this improvement was minimal, i.e., within 5%, and therefore within the measurement error margin. Nevertheless, we could not exclude the possibility that the particle size of the AR_SOL_7 samples had been reduced based on the SEM images, and this could have also been the cause of the increase.

3. Materials and Methods

3.1. Materials

During the study, the following TiO_2 NPs were used: Sigma-Aldrich anatase (AA; 100 wt% anatase) and Sigma-Aldrich rutile (AR; 96 wt% rutile, 4 wt% anatase) (St. Louis, MO, USA). In every instance, ultrapure Millipore Milli-Q water (18.2 MΩ·cm^{-1}) was used. As a model pollutant, we employed phenol (VWR, >99%) to measure the photocatalytic activity.

3.2. Soil Sampling and Analysis

Ten Regosol and ten Solonetz topsoil samples were taken from two distinct locations as part of the soil sampling process. The Solonetz samples were collected from a meadow close to Szatymaz, Hungary, and the Regosol samples were collected from a woodland close to Tallya, Hungary (Figure S1). Then, 0–20 cm depths of topsoil from the levels of 0–10 cm and 10–20 cm were combined. The soil samples were allowed to air dry for ten days before being sieved using a 2 mm sieve. The Supplementary Material section contains

information on the soil parameters (Table S1), which were measured in accordance with the Hungarian Standards (MSZ) and include details of the pH, electrical conductivity (Ec), total salt concentration, texture, and organic matter content [68,69].

3.3. Soil Solution Preparation and Analysis

MQ water was used for soil solution preparation, and the solid-to-solution ratio was 1:2.5. The mixtures were rotated for 17 h; after that, they were centrifuged for 10 min at 4400 rpm and filtered over a 13 µm pore size paper filter.

A digital pH meter (Inolab pH 720) was used to measure the pH of the soil solution, and a conductivity meter (Orion 3-Star, Thermo Electron Corporation (Thermo Fisher, Waltham, MA, USA)) was used to measure the Ec. The ionic strength values (IS) were calculated from the Ec results [12]. The total organic carbon content of the soil solutions (TOC) was measured using Analytik Jena—Multi N/C 2100 S (Analytik Jena GmbH, Jena, Germany).

Inductively coupled plasma optical emission spectroscopy (ICP-OES) using Ar as the carrier gas was performed with a Perkin Elmer Optima 7000DV (PerkinElmer, Inc., Waltham, MA, USA) to assess the major element content (Na, K, Ca, Mg, Al, Fe) of the soil solutions. Using an NH_4Cl buffer at a pH of 8.5 as the reagent, flow injection analysis (FIA) measurements were performed using a Foss FIA Star 5000 spectrometer (FOSS Analytical A/S, Hillerød, Denmark) to ascertain the concentration of NO_3. $SnCl_2$ and $(NH_4)_6Mo_7O_{24}$ were used as reagents for the determination of PO_4. Furthermore, an ion chromatograph (IC) (Dionex ICS-1600 (Thermo Fisher, Sunnyvale, CA, USA)) was utilized to quantify the amounts of F, Cl and SO_4.

3.4. Characterization of TiO_2 NPs

The nanomaterials underwent characterization through several techniques. X-Ray diffraction (XRD) patterns were obtained using a Rigaku Miniflex II diffractometer (Rigaku, Neu-Isenburg, Germany) with Cu-Kα radiation (λ = 1.5406 Å), covering a 2θ range of 20–80° at a scan speed of 1 min^{-1}. Primary crystallite sizes were calculated using the Scherrer equation [70]. Dried powder samples (100 mg) were used for the measurements, which were placed on a glass slide before analysis.

Morphological analysis was performed with a Hitachi S-4700 Type II scanning electron microscope (SEM) (Hitachi Ltd., Hitachi, Tokyo, Japan) after coating the samples with gold NPs (<10 nm). The imaging was carried out under high vacuum conditions using an accelerating voltage of X kV. Secondary electron (SE) and backscattered electron (BSE) detectors were utilized to capture the surface morphology and compositional contrast. Sample preparation involved drying the powders, mounting them on conductive carbon tape, and sputter coating them with gold to prevent charging effects during imaging.

Surface changes were analyzed using a Bruker Equinox 55 infrared spectrometer (IR) (Bruker Corporation, Bremen, Germany), with samples pressed into pellets with KBr powder and IR spectra recorded at a resolution of 2 cm^{-1}. Dried samples were used for the measurements, with approximately 1 mg of the sample finely ground and mixed with KBr in a 1:100 ratio. The mixture was then pressed into transparent pellets under high pressure to ensure uniformity and minimize scattering effects.

The ζ potential of the NPs was measured with a Horiba SZ-100 Nanoparticle Analyzer (Kyoto, Japan) in a carbon electrode cell using the Smoluchowski model for a dispersion concentration of 0.001 *w*/*v*%.

Specs XPS equipment (SPECS Surface Nano Analysis GmbH, Berlin, Germany) with an XR50 dual-anode X-Ray source and a Phoibos 150 hemispherical electron analyzer was used to collect data for X-Ray photoelectron spectroscopy (XPS). Then, 150 W of

electricity were used to run the Al Kα source. To counteract the sample charge during X-Ray irradiation, an electron flood cannon was employed. While the high-resolution spectra were obtained with a pass energy of 20 eV, the survey spectra were obtained with a pass energy of 100 eV. Version 2.3.25 PR1.0.45 of the CasaXPS software was used for the assessment. The inner reference employed was the aliphatic component of the C1s spectra, with a binding energy of 284.8 eV. A Shirley background was used to correct the high-resolution spectra, and a Gauss–Lorentz product function with a 30% Lorentzian contribution was used to match all of the peaks. The relative sensitivity factors derived from Scofield cross sections were applied to adjust the peak area on the survey spectrum, which was used to quantify the elements.

A TiO_2 NPs solution at a concentration of 1 $g \cdot L^{-1}$ was mixed with a phenol solution at an initial concentration (C_0) of 0.1 mM, which was then sonicated for 10 min. Photocatalytic activity was assessed using phenol as a model pollutant at room temperature in an open-top glass reactor. The light source was positioned above the reactor, which was covered with a quartz plate to minimize evaporation. Excitation was achieved with a UV light source (λ_{max} = 364 nm, Vilber-Lourmat T-6L UV-A (Vilber Lourmat, Collégien, France), 6 W), which was then placed 5 cm from the reactor. Throughout the measurements, the suspensions were continuously stirred at 400 rpm. To reach adsorption–desorption equilibrium, the suspension was stirred in the dark for 10 min before turning on the lamps. Throughout the experiments, synthetic air was supplied at a flow rate of 30 L/h while the suspension was continuously stirred, and the temperature was maintained at 25 °C. Phenol concentration was tracked using a high-performance liquid chromatograph (HPLC) equipped with a Merck Hitachi L-4250 UV-vis detector (Hitachi Ltd., Tokyo, Japan) and a Merck Hitachi L-7100 low-pressure pump (Hitachi Ltd., Tokyo, Japan), with a flow rate of 0.7 $cm^3 \cdot min^{-1}$ and a detection wavelength of 210 nm. The eluent used was a 50:50 (v/v) methanol–water mixture. Calibration was carried out using standard solutions of phenol prepared in the same solvent system, covering the expected concentration range.

After HPLC analysis, the degradation percentage (%D) of each sample in a 100 mL aqueous phenol solution with 0.1 mM were obtained with the following:

$$\%D = ((C_o - C_t)/C_o) \times 100, \quad (2)$$

where C_o is the original sample concentration at zero irradiation time and C_t remains at concentration after an irradiation time of 180 min [71].

The data processing, spectrum normalization, and figure preparation were carried out using Origin 2021 software.

3.5. Soil Solution Experiments

Ten pre-prepared soil solutions from Solonetz and Regosol were combined, and a single homogenous sample representative of both Solonetz and Regosol was used for all of the trials. Stock solutions containing 5 $g \cdot L^{-1}$ of TiO_2 NPs (where the AA and AR were kept separate) were prepared using MQ water. Subsequently, the TiO_2-containing soil solutions underwent ten minutes of ultrasonication to prepare the 500 $mg \cdot L^{-1}$ of TiO_2 NP concentration in the soil solutions. The concentration of suspensions utilized was chosen to be comparable to those frequently found in the literature. After the TiO_2 stock suspension was added to the soil solution, the resulting suspension was mixed using a magnetic stirrer. The suspensions were centrifuged for 10 min at 3700 RPM after TiO_2 NPs, and the soil solutions interacted for 4 and 168 h. Using different interaction times is important for understanding both the short-term and long-term effects of TiO_2 NP interactions within soil solutions. The shorter interaction time helps to assess the immediate impact and initial dispersion of the NPs, while the longer durations allow for the observation of changes in

stability, surface chemistry, and potential aggregation over time. This approach provides a more comprehensive understanding of how TiO_2 behaves under varying environmental conditions and durations, reflecting real-world scenarios more accurately.

4. Conclusions

In this study, we investigated the effect of the properties of soil solutions with different chemical parameters on the behavior of anatase and rutile TiO_2 NPs. By analyzing their interactions with the soil solutions from Regosol and Solonetz soils (major differences in pH, ionic strength, and organic matter content), we identified the key factors determining the stability, surface chemistry, and photocatalytic performance of these NPs. Our results showed that interaction time is a critical factor influencing the behavior of TiO_2 NPs. Short-term interactions mainly affected the surface charge and initial dispersion, while long-term exposure resulted in more profound changes in the morphology. Specifically, it resulted in a decrease in primary crystallite size and a possible increase in surface amorphization for the samples exposed to Solonetz soil solution. This result, in turn, calls into question the inert nature of TiO_2 and its stability in the environment. Indeed, once released, these materials become smaller in size over time—this is particularly true for rutile. The smaller size can lead to higher mobility in the soil and is more damaging to living organisms. Changes due to interaction with soil solutions have also been associated with a decrease in photocatalytic activity. This is due to the cumulative effects of surface adsorption, ionic strength-induced aggregation, and structural changes in NP over time. However, it is important to note that the extent of the decrease in activity in our results is strongly influenced by the nature of the soil solutions: while samples that interacted with acidic Regosol soil solutions showed a drastic decrease in activity after a longer interaction time, this was much less pronounced for Solonetz. These results demonstrate how TiO_2 NP behavior in soils is dynamic and complicated, implying that understanding the environmental impact of these nanostructures requires taking into account the particular soil conditions and the length of their exposure. The main emphasis of this work was the dynamic interaction between the material and the chemical composition of the soil solution. Future research will investigate the behavior of TiO_2 NPs in relation to the physical qualities of the soil in an effort to gain a more thorough understanding. By advancing knowledge of the possible dangers connected to TiO_2 NP exposure in soil habitats, this work helps to guarantee environmental sustainability by directing efforts to lessen the negative impacts of the exposure.

Supplementary Materials: The following supporting information can be downloaded at: https://www.mdpi.com/article/10.3390/catal15020190/s1, Figure S1: The location of the sampling areas; Table S1: The basic parameters of the soil samples (The references [68,69,72] are cited in the Supplemental Materials).

Author Contributions: K.S.: conceptualization, investigation, writing—original draft, and formal analysis. Á.Á.: investigation. T.G.: investigation. L.S.: investigation. M.T.: investigation. Á.K.: resources and funding acquisition. Z.K.: resources and funding acquisition. Z.P.: conceptualization, writing—review and editing, supervision, and funding acquisition. All authors have read and agreed to the published version of the manuscript.

Funding: The authors would like to express their gratitude for the financial support provided by the 2021-1.2.6-TÉT-IPARI-MA-2022-00009 project. T. Gyulavári acknowledges the Bolyai János scholarship (BO/00447/23) provided by the Hungarian Academy of Sciences. TKP2021-NVA-19 was implemented with the support provided by the Ministry of Innovation and Technology of Hungary from the National Research, Development and Innovation Fund, which was financed under the TKP2021-NVA funding scheme. Áron Ágoston acknowledges the Doctoral Student Scholarship Program of the Co-operative Doctoral Program (EKÖP-KDP-24-SZTE-6) of the Ministry of Innovation and Technology, which was financed from the National Research, Development and Innovation Fund.

Data Availability Statement: Data are contained within the article or in the Supplementary Material section.

Conflicts of Interest: The authors declare no conflicts of interest.

Abbreviations

The following abbreviations are used in this manuscript:

AA_REF	Pure/reference Aldrich anatase
AA_AP	Aldrich anatase after phenol degradation
AA_REG_4	Aldrich anatase after interaction with Regosol soil solution for 4 h
AA_REG_4_AP	Aldrich anatase after interaction with Regosol soil solution for 4 h and phenol degradation
AA_REG_7	Aldrich anatase after interaction with Regosol soil solution for 168 h
AA_REG_7_AP	Aldrich anatase after interaction with Regosol soil solution for 168 h and phenol degradation
AA_SOL_4	Aldrich anatase after interaction with Solonetz soil solution for 4 h
AA_SOL_4_AP	Aldrich anatase after interaction with Solonetz soil solution for 4 h and phenol degradation
AA_SOL_7	Aldrich anatase after interaction with Solonetz soil solution for 168 h
AA_SOL_7_AP	Aldrich anatase after interaction with Solonetz soil solution for 168 h and phenol degradation
AR_REF	Pure/reference Aldrich rutile
AR_AP	Aldrich rutile after phenol degradation
AR_REG_4	Aldrich rutile after interaction with Regosol soil solution for 4 h
AR_REG_4_AP	Aldrich rutile after interaction with Regosol soil solution for 4 h and phenol degradation
AR_REG_7	Aldrich rutile after interaction with Regosol soil solution for 168 h
AR_REG_7_AP	Aldrich rutile after interaction with Regosol soil solution for 168 h and phenol degradation
AR_SOL_4	Aldrich rutile after interaction with Solonetz soil solution for 4 h
AR_SOL_4_AP	Aldrich rutile after interaction with Solonetz soil solution for 4 h and phenol degradation
AR_SOL_7	Aldrich rutile after interaction with Solonetz soil solution for 168 h
AR_SOL_7_AP	Aldrich rutile after interaction with Solonetz soil solution for 168 h and phenol degradation

References

1. Reli, M.; Nadrah, P.; Filip Edelmannová, M.; Ricka, R.; Sever Škapin, A.; Lavrenčič Štangar, U.; Kočí, K. Photocatalytic CO_2 reduction over mesoporous TiO_2 photocatalysts. *Mater. Sci. Semicond. Process.* **2024**, *169*, 107927. [CrossRef]
2. Ayappan, C.; Xing, R.; Zhang, X.; Luo, D.; Liu, S.; Fujishima, A. TiO_2-based photocatalysts for emerging gaseous pollutants removal: From photocatalysts to reactors design. *Coord. Chem. Rev.* **2024**, *515*, 215960. [CrossRef]
3. Kato, K.; Matsui, R.; Xin, Y.; Xu, Y.; Shirai, T. Fast synthesis of Ti3+ self-doped TiO_2/few-layer graphene oxide core/shell nanoparticles for sustainable photocatalytic water purification. *Appl. Surf. Sci.* **2024**, *664*, 160280. [CrossRef]
4. Reddy, N.A.; Panchangam, S.C. Evaluation of self-cleaning performance of TiO_2-intermixed and TiO_2-coated cement mortars under natural sunlight. *J. Sustain. Cem.-Based Mater.* **2024**, *13*, 1032–1049. [CrossRef]
5. Ayar, P.; Ruhi, A.; Baibordy, A.; Asadi Azadgoleh, M.; Mohammadi, M.M.; Abdipour, S.V. Toward sustainable roads: A critical review on nano-TiO_2 application in asphalt pavement. *Innov. Infrastruct. Solut.* **2024**, *9*, 148. [CrossRef]
6. Hsu, C.-Y.; Mahmoud, Z.H.; Abdullaev, S.; Ali, F.K.; Ali Naeem, Y.; Mzahim Mizher, R.; Morad Karim, M.; Abdulwahid, A.S.; Ahmadi, Z.; Habibzadeh, S.; et al. Nano titanium oxide (nano-TiO_2): A review of synthesis methods, properties, and applications. *Case Stud. Chem. Environ. Eng.* **2024**, *9*, 100626. [CrossRef]
7. Tesser, M.E.; Guilger, M.; Bilesky-José, N.; Risso, W.E.; de Lima, R.; Martinez, C.B.d.R. Biogenic metallic nanoparticles (Ag, TiO_2, Fe) as potential fungicides for agriculture: Are they safe for the freshwater mussel Anodontites trapesialis? *Chemosphere* **2022**, *309*, 136664. [CrossRef]
8. Selva Esakki, E.; Deepa, G.; Vivek, P.; Meenakshi Sundar, S. Investigation of TiO_2 as photoanode for solar cell application. *Solid State Commun.* **2023**, *371*, 115266. [CrossRef]
9. Baranowska-Wójcik, E.; Rymuszka, A.; Sierosławska, A.; Szwajgier, D. Effect of Food Additive E171 and Titanium Dioxide Nanoparticles (TiO2-NPs) on Caco-2 Colon Cancer Cells. *Appl. Sci.* **2024**, *14*, 9387. [CrossRef]
10. Eddy, D.R.; Permana, M.D.; Sakti, L.K.; Sheha, G.A.N.; Solihudin; Hidayat, S.; Takei, T.; Kumada, N.; Rahayu, I. Heterophase Polymorph of TiO_2 (Anatase, Rutile, Brookite, TiO_2 (B)) for Efficient Photocatalyst: Fabrication and Activity. *Nanomaterials* **2023**, *13*, 704. [CrossRef]
11. Mutsak Ahmed, R.; Hasan, I. A review on properties and applications of TiO_2 and associated nanocomposite materials. *Mater. Today Proc.* **2023**, *81*, 1073–1078. [CrossRef]

12. Solymos, K.; Babcsányi, I.; Ariya, B.; Gyulavári, T.; Ágoston, Á.; Szamosvölgyi, Á.; Kukovecz, Á.; Kónya, Z.; Farsang, A.; Pap, Z. Photocatalytic and surface properties of titanium dioxide nanoparticles in soil solutions. *Environ. Sci. Nano* **2024**, *11*, 1204–1216. [CrossRef]
13. Gyulavári, T.; Pap, Z.; Kovács, G.; Baia, L.; Todea, M.; Hernádi, K.; Veréb, G. Peroxo group enhanced nanorutile as visible light active photocatalyst. *Catal. Today* **2017**, *284*, 129–136. [CrossRef]
14. Di Paola, A.; Bellardita, M.; Palmisano, L. Brookite, the Least Known TiO_2 Photocatalyst. *Catalysts* **2013**, *3*, 36–73. [CrossRef]
15. Shah, S.N.A.; Shah, Z.; Hussain, M.; Khan, M. Hazardous Effects of Titanium Dioxide Nanoparticles in Ecosystem. *Bioinorg. Chem. Appl.* **2017**, *2017*, 4101735. [CrossRef]
16. Baranowska-Wójcik, E.; Szwajgier, D.; Oleszczuk, P.; Winiarska-Mieczan, A. Effects of Titanium Dioxide Nanoparticles Exposure on Human Health-a Review. *Biol. Trace Elem. Res.* **2020**, *193*, 118–129. [CrossRef]
17. Tanu, M. Nano TiO_2-Based Smart Superhydrophilic Self-Cleaning Surfaces. In *Photocatalysts*; Nasser, S.A., Saleh Saeed, A., Ahmed, A., Eds.; IntechOpen: Rijeka, Croatia, 2022; Chapter 4; pp. 1–10.
18. Turner, A.; Filella, M. The role of titanium dioxide on the behaviour and fate of plastics in the aquatic environment. *Sci. Total Environ.* **2023**, *869*, 161727. [CrossRef] [PubMed]
19. Wahab, A.; Muhammad, M.; Ullah, S.; Abdi, G.; Shah, G.M.; Zaman, W.; Ayaz, A. Agriculture and environmental management through nanotechnology: Eco-friendly nanomaterial synthesis for soil-plant systems, food safety, and sustainability. *Sci. Total Environ.* **2024**, *926*, 171862. [CrossRef]
20. Manzoor, Q.; Sajid, A.; Ali, Z.; Nazir, A.; Sajid, A.; Imtiaz, F.; Iqbal, S.; Younas, U.; Arif, H.; Iqbal, M. Toxicity spectrum and detrimental effects of titanium dioxide nanoparticles as an emerging pollutant: A review. *Desalination Water Treat.* **2024**, *317*, 100025. [CrossRef]
21. Moll, J.; Klingenfuss, F.; Widmer, F.; Gogos, A.; Bucheli, T.D.; Hartmann, M.; van der Heijden, M.G.A. Effects of titanium dioxide nanoparticles on soil microbial communities and wheat biomass. *Soil Biol. Biochem.* **2017**, *111*, 85–93. [CrossRef]
22. Larue, C.; Khodja, H.; Herlin-Boime, N.; Brisset, F.; Flank, A.M.; Fayard, B.; Chaillou, S.; Carrière, M. Investigation of titanium dioxide nanoparticles toxicity and uptake by plants. *J. Phys. Conf. Ser.* **2011**, *304*, 012057. [CrossRef]
23. Skocaj, M.; Filipic, M.; Petkovic, J.; Novak, S. Titanium dioxide in our everyday life; is it safe? *Radiol. Oncol.* **2011**, *45*, 227–247. [CrossRef]
24. Czekes, Z.; Bai, D.; Vincze, J.; Gál, E.; Réthi-Nagy, Z.; Baia, L.; Pap, Z. Commercial photocatalyst changes the behavior of Formica pratensis and Formica polyctena. *Environ. Sci. Nano* **2023**, *10*, 72–79. [CrossRef]
25. Simonin, M.; Guyonnet, J.P.; Martins, J.M.F.; Ginot, M.; Richaume, A. Influence of soil properties on the toxicity of TiO_2 nanoparticles on carbon mineralization and bacterial abundance. *J. Hazard. Mater.* **2015**, *283*, 529–535. [CrossRef]
26. Buchanan, J.R. 3.13—Decentralized Wastewater Treatment. In *Comprehensive Water Quality and Purification, Ahuja, S., Ed.*; Elsevier: Waltham, MA, USA, 2014; pp. 244–267.
27. Sparks, D.L.; Singh, B.; Siebecker, M.G. Chapter 1—An Introduction to Environmental Soil Chemistry. In *Environmental Soil Chemistry*, 3rd ed.; Sparks, D.L., Singh, B., Siebecker, M.G., Eds.; Academic Press: Boston, MA, USA, 2024; pp. 1–38.
28. Simonin, M.; Martins, J.M.F.; Uzu, G.; Spadini, L.; Navel, A.; Richaume, A. Low mobility of CuO and TiO_2 nanoparticles in agricultural soils of contrasting texture and organic matter content. *Sci. Total Environ.* **2021**, *783*, 146952. [CrossRef] [PubMed]
29. Lucian, R.; Nicolae, G.; Mărăcineanu, L. *The Analysis of Physical and Chemical Properties of Regosol from Brădești, Dolj County*; Annals of the University of Cariova: Craiova, Romania, 2021; Volume XXV (LXI), pp. 190–195.
30. Hopmans, J.W.; Qureshi, A.S.; Kisekka, I.; Munns, R.; Grattan, S.R.; Rengasamy, P.; Ben-Gal, A.; Assouline, S.; Javaux, M.; Minhas, P.S.; et al. Chapter One—Critical knowledge gaps and research priorities in global soil salinity. In *Advances in Agronomy*; Sparks, D.L., Ed.; Academic Press: Cambridge, MA, USA, 2021; Volume 169, pp. 1–191.
31. Verhovšek, D.; Veronovski, N.; Lavrenčič Štangar, U.; Kete, M.; Žagar, K.; Čeh, M. The Synthesis of Anatase Nanoparticles and the Preparation of Photocatalytically Active Coatings Based on Wet Chemical Methods for Self-Cleaning Applications. *Int. J. Photoenergy* **2012**, *2012*, 329796. [CrossRef]
32. Hanaor, D.; Michelazzi, M.; Veronesi, P.; Leonelli, C.; Romagnoli, M.; Sorrell, C. Anodic aqueous electrophoretic deposition of titanium dioxide using carboxylic acids as dispersing agents. *J. Eur. Ceram. Soc.* **2011**, *31*, 1041–1047. [CrossRef]
33. Gentili, D.; Ori, G. Reversible assembly of nanoparticles: Theory, strategies and computational simulations. *Nanoscale* **2022**, *14*, 14385–14432. [CrossRef]
34. Hedberg, J.; Blomberg, E.; Odnevall Wallinder, I. In the Search for Nanospecific Effects of Dissolution of Metallic Nanoparticles at Freshwater-Like Conditions: A Critical Review. *Environ. Sci. Technol.* **2019**, *53*, 4030–4044. [CrossRef]
35. Mathew, R.A.; Wu, G.; Zhang, Y.; Shakiba, S.; Yao, Y.; Tsai, A.-L.; Louie, S.M. Natural organic matter adsorption conditions influence photocatalytic reaction pathways of phosphate-treated titanium dioxide nanoparticles. *Environ. Sci. Nano* **2021**, *8*, 2165–2176. [CrossRef]
36. Ye, Y.; Bruning, H.; Liu, W.; Rijnaarts, H.; Yntema, D. Effect of dissolved natural organic matter on the photocatalytic micropollutant removal performance of TiO_2 nanotube array. *J. Photochem. Photobiol. A Chem.* **2019**, *371*, 216–222. [CrossRef]

37. Jiang, D.; Otitoju, T.A.; Ouyang, Y.; Shoparwe, N.F.; Wang, S.; Zhang, A.; Li, S. A Review on Metal Ions Modified TiO_2 for Photocatalytic Degradation of Organic Pollutants. *Catalysts* **2021**, *11*, 1039. [CrossRef]
38. Nolan, M. Electronic coupling in iron oxide-modified TiO_2 leads to a reduced band gap and charge separation for visible light active photocatalysis. *Phys. Chem. Chem. Phys.* **2011**, *13*, 18194–18199. [CrossRef] [PubMed]
39. Sakar, M.; Mithun Prakash, R.; Do, T.-O. Insights into the TiO_2-Based Photocatalytic Systems and Their Mechanisms. *Catalysts* **2019**, *9*, 680. [CrossRef]
40. Ambrus, Z.; Balázs, N.; Alapi, T.; Wittmann, G.; Sipos, P.; Dombi, A.; Mogyorósi, K. Synthesis, structure and photocatalytic properties of Fe(III)-doped TiO_2 prepared from $TiCl_3$. *Appl. Catal. B Environ.* **2008**, *81*, 27–37. [CrossRef]
41. Krivec, M.; Dillert, R.; Bahnemann, D.W.; Mehle, A.; Štrancar, J.; Dražić, G. The nature of chlorine-inhibition of photocatalytic degradation of dichloroacetic acid in a TiO_2-based microreactor. *Phys. Chem. Chem. Phys.* **2014**, *16*, 14867–14873. [CrossRef] [PubMed]
42. Shih, Y.H.; Liu, W.S.; Su, Y.F. Aggregation of stabilized TiO_2 nanoparticle suspensions in the presence of inorganic ions. *Environ. Toxicol. Chem.* **2012**, *31*, 1693–1698. [CrossRef] [PubMed]
43. French, R.A.; Jacobson, A.R.; Kim, B.; Isley, S.L.; Penn, R.L.; Baveye, P.C. Influence of Ionic Strength, pH, and Cation Valence on Aggregation Kinetics of Titanium Dioxide Nanoparticles. *Environ. Sci. Technol.* **2009**, *43*, 1354–1359. [CrossRef] [PubMed]
44. Farner Budarz, J.; Turolla, A.; Piasecki, A.F.; Bottero, J.-Y.; Antonelli, M.; Wiesner, M.R. Influence of Aqueous Inorganic Anions on the Reactivity of Nanoparticles in TiO_2 Photocatalysis. *Langmuir* **2017**, *33*, 2770–2779. [CrossRef] [PubMed]
45. Ziemniak, S.E.; Jones, M.E.; Combs, K.E.S. Solubility behavior of titanium(IV) oxide in alkaline media at elevated temperatures. *J. Solut. Chem.* **1993**, *22*, 601–623. [CrossRef]
46. Li, W.; Liang, R.; Hu, A.; Huang, Z.; Zhou, Y.N. Generation of oxygen vacancies in visible light activated one-dimensional iodine TiO_2 photocatalysts. *RSC Adv.* **2014**, *4*, 36959–36966. [CrossRef]
47. Lowry, G.V.; Hill, R.J.; Harper, S.; Rawle, A.F.; Hendren, C.O.; Klaessig, F.; Nobbmann, U.; Sayre, P.; Rumble, J. Guidance to improve the scientific value of zeta-potential measurements in nanoEHS. *Environ. Sci. Nano* **2016**, *3*, 953–965. [CrossRef]
48. Kaliannan, N.K.; Krishnamurthy, K. Computational study on the structural and surface properties of amorphous hydroxylated TiO_2 spherical nanoparticles. *J. Nanoparticle Res.* **2017**, *19*, 346. [CrossRef]
49. Waegele, M.M.; Gunathunge, C.M.; Li, J.; Li, X. How cations affect the electric double layer and the rates and selectivity of electrocatalytic processes. *J. Chem. Phys.* **2019**, *151*, 160902. [CrossRef]
50. Ignatchenko, A.V.; Denman, P.E. Mapping Acid–Base Sites on Anatase Titania (100) and (101) Surfaces by Density Functional Theory: The Link Between Lewis Acidity and the Surface Ability to Flex. *Surfaces* **2024**, *7*, 1060–1078. [CrossRef]
51. Luttrell, T.; Halpegamage, S.; Tao, J.; Kramer, A.; Sutter, E.; Batzill, M. Why is anatase a better photocatalyst than rutile?—Model studies on epitaxial TiO_2 films. *Sci. Rep.* **2014**, *4*, 4043. [CrossRef] [PubMed]
52. Gohari, G.; Mohammadi, A.; Akbari, A.; Panahirad, S.; Dadpour, M.R.; Fotopoulos, V.; Kimura, S. Titanium dioxide nanoparticles (TiO_2 NPs) promote growth and ameliorate salinity stress effects on essential oil profile and biochemical attributes of Dracocephalum moldavica. *Sci. Rep.* **2020**, *10*, 912. [CrossRef]
53. Azzolina-Jury, F.; Thibault-Starzyk, F. Mechanism of Low Pressure Plasma-Assisted CO_2 Hydrogenation Over Ni-USY by Microsecond Time-resolved FTIR Spectroscopy. *Top. Catal.* **2017**, *60*, 1709–1721. [CrossRef]
54. Abbas, O.; Compère, G.; Larondelle, Y.; Pompeu, D.; Rogez, H.; Baeten, V. Phenolic compound explorer: A mid-infrared spectroscopy database. *Vib. Spectrosc.* **2017**, *92*, 111–118. [CrossRef]
55. Beljebbar, A.; Dukic, S.; Amharref, N.; Bellefqih, S.; Manfait, M. Monitoring of Biochemical Changes through the C6 Gliomas Progression and Invasion by Fourier Transform Infrared (FTIR) Imaging. *Anal. Chem.* **2009**, *81*, 9247–9256. [CrossRef] [PubMed]
56. Gyulavári, T.; Veréb, G.; Pap, Z.; Réti, B.; Baan, K.; Todea, M.; Magyari, K.; Szilágyi, I.M.; Hernadi, K. Utilization of Carbon Nanospheres in Photocatalyst Production: From Composites to Highly Active Hollow Structures. *Materials* **2019**, *12*, 2537. [CrossRef] [PubMed]
57. Kovács, G.; Baia, L.; Vulpoi, A.; Radu, T.; Karácsonyi, É.; Dombi, A.; Hernádi, K.; Danciu, V.; Simon, S.; Pap, Z. $TiO_2/WO_3/Au$ nanoarchitectures' photocatalytic activity, "from degradation intermediates to catalysts' structural peculiarities", Part I: Aeroxide P25 based composites. *Appl. Catal. B Environ.* **2014**, *147*, 508–517. [CrossRef]
58. Machado, W.; Franchini, J.C.; de Fátima Guimarães, M.; Filho, J.T. Spectroscopic characterization of humic and fulvic acids in soil aggregates, Brazil. *Heliyon* **2020**, *6*, e04078. [CrossRef]
59. Dovbeshko, G.I.; Gridina, N.Y.; Kruglova, E.B.; Pashchuk, O.P. FTIR spectroscopy studies of nucleic acid damage. *Talanta* **2000**, *53*, 233–246. [CrossRef]
60. Lu, H.-l.; Nkoh, J.N.; Abdulaha-Al Baquy, M.; Dong, G.; Li, J.-y.; Xu, R.-k. Plants alter surface charge and functional groups of their roots to adapt to acidic soil conditions. *Environ. Pollut.* **2020**, *267*, 115590. [CrossRef] [PubMed]
61. Dreissig, I.; Machill, S.; Salzer, R.; Krafft, C. Quantification of brain lipids by FTIR spectroscopy and partial least squares regression. *Spectrochim. Acta Part A Mol. Biomol. Spectrosc.* **2009**, *71*, 2069–2075. [CrossRef]

62. Schwan, R.; Kaufmann, M.; Leicht, D.; Schwaab, G.; Havenith, M. Infrared spectroscopy of the ν2 band of the water monomer and small water clusters (H2O)n=2,3,4 in helium droplets. *Phys. Chem. Chem. Phys.* **2016**, *18*, 24063–24069. [CrossRef]
63. Fu, H.; Lin, J.; Shang, G.; Dong, W.; Grassian, V.H.; Carmichael, G.R.; Li, Y.; Chen, J. Solubility of Iron from Combustion Source Particles in Acidic Media Linked to Iron Speciation. *Environ. Sci. Technol.* **2012**, *46*, 11119–11127. [CrossRef]
64. Kovács, G.; Pap, Z.; Coteț, C.; Coșoveanu, V.; Baia, L.; Danciu, V. Photocatalytic, Morphological and Structural Properties of the TiO_2-SiO_2-Ag Porous Structures Based System. *Materials* **2015**, *8*, 1059–1073. [CrossRef]
65. Jayalath, S.; Wu, H.; Larsen, S.C.; Grassian, V.H. Surface Adsorption of Suwannee River Humic Acid on TiO_2 Nanoparticles: A Study of pH and Particle Size. *Langmuir* **2018**, *34*, 3136–3145. [CrossRef] [PubMed]
66. Mange, F.; Couchot, P.; Foissy, A.; Pierre, A. Effects of Sodium and Calcium Ions on the Aggregation of Titanium Dioxide, at High pH, in Aqueous Dispersions. *J. Colloid Interface Sci.* **1993**, *159*, 58–67. [CrossRef]
67. Loganathan, N.; Ferguson, B.O.; Arey, B.; Argersinger, H.E.; Bowers, G.M. A Mechanistic Exploration of Natural Organic Matter Aggregation and Surface Complexation in Smectite Mesopores. *J. Phys. Chem. A* **2020**, *124*, 9832–9843. [CrossRef]
68. Pham, N.T.H.; Babcsányi, I.; Balling, P.; Farsang, A. Accumulation patterns and health risk assessment of potentially toxic elements in the topsoil of two sloping vineyards (Tokaj-Hegyalja, Hungary). *J. Soils Sediments* **2022**, *22*, 2671–2689. [CrossRef]
69. Pham, N.T.H.; Babcsányi, I.; Farsang, A. Ecological risk and enrichment of potentially toxic elements in the soil and eroded sediment in an organic vineyard (Tokaj Nagy Hill, Hungary). *Environ. Geochem. Health* **2022**, *44*, 1893–1909. [CrossRef] [PubMed]
70. Uvarov, V.; Popov, I. Metrological characterization of X-Ray diffraction methods for determination of crystallite size in nano-scale materials. *Mater. Charact.* **2007**, *58*, 883–891. [CrossRef]
71. Karami, M.; Ghanbari, M.; Amiri, O.; Salavati-Niasari, M. Enhanced antibacterial activity and photocatalytic degradation of organic dyes under visible light using cesium lead iodide perovskite nanostructures prepared by hydrothermal method. *Sep. Purif. Technol.* **2020**, *253*, 117526. [CrossRef]
72. Manaljav, S.; Farsang, A.; Barta, K.; Tobak, Z.; Juhász, S.; Balling, P.; Babcsányi, I. The Impact of Soil Erosion on the Spatial Distribution of Soil Characteristics and Potentially Toxic Element Contents in a Sloping Vineyard in Tállya, Ne Hungary. *J. Environ. Geogr.* **2021**, *14*, 47–57. [CrossRef]